J Mater Sci (2018) 53:4693–4704

Polymers

Microscopic investigation of polyacrylonitrile fiber fibrils separated by ultrasonic etching

Christina Kunzmann[1,*], Gregor Schmidt-Bilkenroth[1], Judith Moosburger-Will[2], and Siegfried Horn[1,2]

[1] *Experimental Physics II, Institute of Physics, University of Augsburg, 86135 Augsburg, Germany*
[2] *Institute of Materials Resource Management, University of Augsburg, 86135 Augsburg, Germany*

Received: 6 October 2017
Accepted: 21 November 2017
Published online: 28 November 2017

ABSTRACT

In this study, we analyzed the fibril morphology of different polyacrylonitrile fibers, i.e., two fibers for technical and one for textile applications. The fibers are separated into their fibrils by an ultrasonic etching procedure. For all types of polyacrylonitrile fibers, two different fibril morphologies are found. On the one hand, fibrils with a smooth surface and a homogeneous, amorphous volume structure exist. On the other hand, for the first time in polyacrylonitrile fibers, fibrils with a shish-kebab structure are found. Such fibrils are characterized by a rough surface structure resulting from crystalline lamellar layers oriented perpendicular to a centered shish. With increasing crystallinity of the polyacrylonitrile fibers, the relative amount of shish-kebab fibrils increases. Based on these investigations, a model for the PAN fiber is presented, describing the difference of structure of the two types of fibrils.

Introduction

Polyacrylonitrile (PAN) is a semicrystalline thermoplast and the basis for a variety of products, e.g., membranes for ultrafiltration or fibers [1, 2]. The fiber industry uses PAN as material for textile applications, as hollow fibers for osmosis or—copolymerized with suitable monomers—as precursor fiber for the production of carbon fibers [2]. PAN fibers are the most important precursor material for the production of carbon fibers of high tensile strength [3, 4]. Due to the growing field of applications of carbon fiber-reinforced composite materials, the demand for carbon fibers is increasing and the optimization of fiber properties is in the focus of research [5–7]. Here, in particular the relationship between the parameters of the carbon fiber production process, the evolution of chemical and physical structure of the fibers during the thermal transformation from PAN to carbon and the resulting carbon fiber mechanical parameters are of high interest [8–14]. It is assumed that the prerequisite for a high-quality carbon fiber is a copolymerized PAN precursor fiber with optimally adapted chemical and physical structure, which is mainly defined by the polymerization and spinning process [15–17].

The PAN fiber can be formed using different types of spinning processes [2]. Wet spinning is the common production method for the manufacturing of tows with a large number of filaments [17]. It starts

Address correspondence to E-mail: christina.kunzmann@physik.uni-augsburg.de

https://doi.org/10.1007/s10853-017-1858-z

with the spinning of the PAN solution through a spinneret into a coagulation bath, followed by repeated steps of washing and stretching, and ends with the application of a textile finish agent and drying of the fibers [2, 18]. In this process, the coagulation is one of the most important steps determining the physical structure of the fiber. The parameters of the coagulation process, like chemical composition and temperature of the coagulation bath, control the formation of the micro- and nanostructure of the fiber [19, 20]. Depending on the conditions within the coagulation bath, a spinodal decomposition of the PAN polymer solution in two phases can occur [21, 22]. This results in a gel network, in which the polymer-rich phase forms the bulk of the fiber with the typical fibrillar substructure [23], while the solvent-rich phase results in voids [2, 24]. The fibrils, which typically have diameters of 5–400 nm, are dominantly oriented along the fiber axis [25, 26]. The fibrils consist of PAN molecule chains with a preferred orientation, resulting from the flow of the dilute PAN solution through the spinneret and the stretching of the thus resulting fiber [27, 28]. Long range order of the flexible PAN molecule chains occurs, which is described in literature by different models [29, 30]. The fringed-micelle model describes the formation of small crystallites by the partial alignment of several individual chains [31, 32]. Ref. [33] proposes that polymer chains fold several times to form crystallites. A planar crystal growth of such aligned chains results in a lamellar structure [34, 35]. Depending on the processing conditions, many polymers crystallize in complex lamellae-based structures, like spherulites or shish-kebab structures [35–39]. While spherulites consist of radially oriented lamellae, lamellae of a shish-kebab structure are oriented perpendicular with respect to centered parallel oriented molecular chains (shish) [36–39]. In these complex lamellae-based structures, the folding of the polymer chains within the lamellae is less organized than in polymer single crystals [38]. The folding of the polymer chain can be described by the so-called adjacent chain-folding model, where the molecule chains fold in a regular manner to form a lamella, or by the switchboard-model, where loops, cilia, and tie molecules are assumed to coexist [40–42]. These loops, cilia, tie molecules, and the irregular chain-folding on the fringes of the lamellae form amorphous areas around the crystallites, resulting in an overall semicrystalline material. The orientation of the PAN molecules relative to each other and along the fiber axis, which influences the mechanical properties of the fibers, increases by stretching the fibers during the spinning process [16, 17, 43].

The fibrillar substructure of the PAN fibers and the nanostructure of these fibrils are important for a fundamental understanding of PAN fiber properties, because they influence the properties of the resulting carbon fibers [44]. Microscopy of the surface of PAN fibers offers information about the diameter of surface fibrils and their orientation relative to the fiber axis, as well as of size and morphology of their nanostructures. Information about the volume structure of the PAN fibers can be obtained by fibril separation using an etching process, which also allows detailed investigation of the nanostructure of bulk fibrils [29, 45–47]. Fibril separation by ultrasonic etching applying a suitable solvent solution has become a widely accepted preparation method for different types of fibers [48–54]. Reference [29] for the first time applied an ultrasonic etching process to PAN fibers and described a fibril structure composed of periodically arranged transverse bands. However, the transmission electron microscope (TEM) image shown is of low resolution and, due to the shrinkage of the polymer fibril under the electron beam, diffuse. Wang et al. report a similar form of fibrils and describe the transverse bands as lamellae and the observed fibril morphology as shish-kebab structure without a visible shish [45, 46]. In addition to such fibrils with lamellar surface structure also fibrils with a smooth surface structure are found, which seem to be similar to fibrils investigated without ultrasonic etching process [45, 46].

Here, we investigate the fibrillar micro- and nanostructure of different types of PAN fibers, i.e., two PAN fibers originating from a technical production process and one textile PAN fiber. The fibers were separated into their fibrils by ultrasonic etching. The resulting microscale fibril morphologies were characterized by field emission scanning electron microscopy (FESEM). Nanoscale analysis of the different PAN fibrils was performed by high-resolution atomic force microscopy (AFM) in tapping mode and TEM. Based on this analysis, a model of the volume structure of PAN fibers is presented.

Materials and methods

Polyacrylonitrile fibers and fibril preparation

The fibril structures of three different types of PAN fibers (PAN A, PAN B and PAN C) are analyzed. PAN A and B are technical precursor fibers for the production of carbon fibers with high tensile strengths, and PAN C is a fiber for textile applications. PAN A results from a research project, PAN B is a precursor fiber by Bluestar and PAN C is a textile fiber by Dralon. To analyze the bulk structure, these fibers were separated into their fibrils by ultrasonic etching. To this end, the PAN fibers were cut into pieces with a length of 2–3 mm and were processed in dimethyl sulfoxide (DMSO) solution at a temperature of 75 °C in an ultrasonic bath (USB) (Bandelin Sonorex digitec, frequency of 35 kHz). The set temperature of 75 °C is below the glass transition temperatures of the fibers of 100–120 °C. The concentration of the DMSO solution and the ultrasonic treatment time necessary for fibril separation were found to depend on the PAN fiber type and are discussed in the experimental part of this paper. The resulting PAN dispersions were filtered using a TEM lacey carbon grid, washed with distilled water and dried at room temperature.

Scanning electron microscopy

The samples for FESEM measurements were coated with a thin platinum layer, to guarantee high electrical conductivity of the surface. A FESEM LEO Gemini 982 FEG from Zeiss AG at an acceleration voltage of 1 kV was used. TEM investigation of uncoated fibrils was performed using a JEOL JEM-2100F at an accelerating voltage of 200 keV.

Atomic force microscopy

AFM measurements were carried out using a Dimension Icon atomic force microscope (Bruker). They were performed using the tapping mode with super sharp EBD-SSS NCHR AFM probes from Nanotools with a tip radius of 2–3 nm at a scan rate of 0.5 Hz. The scanning area of the images was 1 μm × 1 μm (512 × 512 pixels). The images were processed and analyzed by the software Nanoscope Analysis v1.40.

X-ray diffraction

X-ray diffraction (XRD) investigations were performed at a Seifert 3003 PTS XRD diffractometer with copper anode. The crystallinity, the crystallite size and the orientation of the crystallites were determined according to Ref. [55].

Results

Microscale surface analysis of fibrils by FESEM

The FESEM investigation demonstrates that the technical PAN fiber A can be successfully separated into fibrils by ultrasonic etching. We find separated material with fragments of the original fiber still preserved after the USB etching. Some of the fibrils are partially connected to the surface of this fiber fragment and are flaking off in bundles (see Fig. 1a). These fibril bundles are of different thickness and are composed of a multitude of individual fibrils with a smooth surface, similar to those of Refs. [45, 46]. In addition, completely separated bundles of smooth fibrils are found. Figure 1b shows these individual fibrils in higher magnification. Evaluation of 1017 individual smooth fibrils results in an average diameter of 65 ± 36 nm, which is in good agreement with the size of smooth fibrils reported by Refs. [25, 45, 46].

In addition to the described smooth fibrils, a second type of fibril with a completely different, rough surface structure (Fig. 1c) is found. In agreement with the rough fibrils described by Refs. [29, 45, 46], the surface structure of these fibrils is characterized by thin lamella-like layers oriented perpendicular to the fibril axis. However, while the rough fibrils described by Refs. [29, 45, 46] have a lamellar, closely packed structure, the lamella-like layers described in this work are arranged more loosely. In Fig. 1d, this rough surface structure of three individual fibrils is shown in higher magnification. The image illustrates that the complete fibril is characterized by a fine porous network of thin layers, which are dominantly oriented perpendicular to the fibril axis. The thin layers are interconnected and show an average thickness of 28 ± 11 nm (evaluation of 126 layers). The average diameter of the complete rough fibrils amounts to 280 ± 115 nm (evaluation of 100 fibrils),

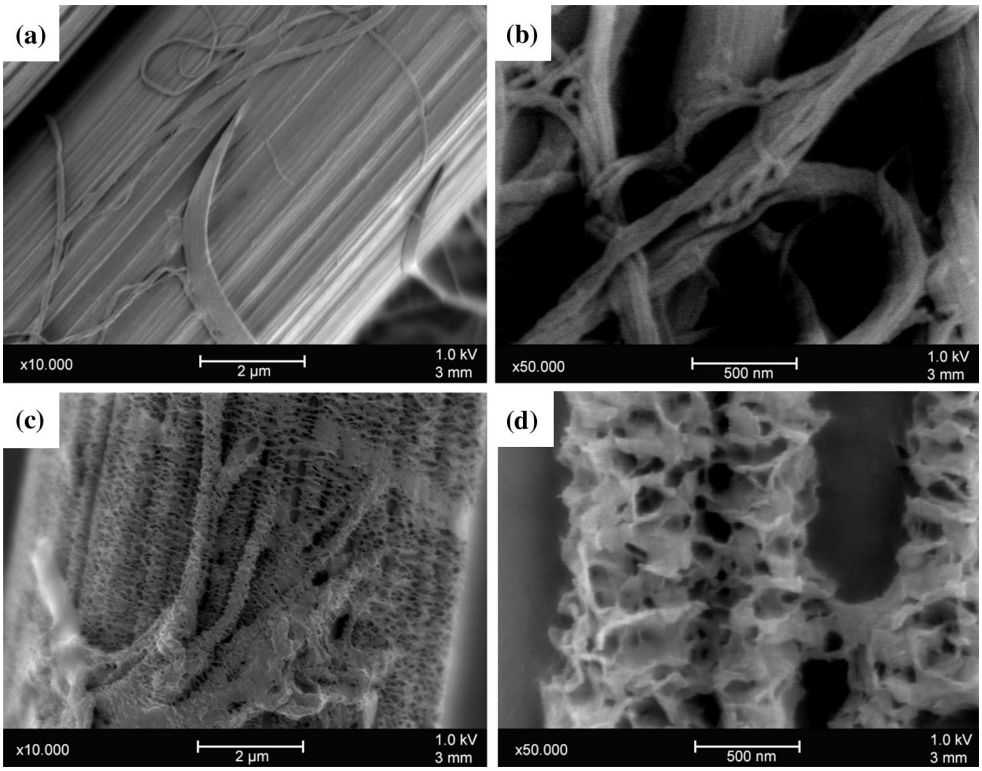

Figure 1 FESEM images of the two different morphologies of PAN fibrils (**a**, **b**) type I: smooth fibrils (**c**, **d**) type II: fibrils with lamella-like microstructures.

which is significantly larger than the average diameter of the smooth fibrils.

Based on these distinctive differences, the described two types of fibrils are classified as type I (smooth fibril) and type II (rough fibril).

Figure 2 shows a region of the fiber characterized by fibrils of type II interpreted as different stages of the solvation process. The images indicate that the lamella-like microstructure of fibrils of type II is carved out during the etching procedure. Figure 2a shows the PAN fiber surface at an early state of the etching process. The fibrillar substructure is visible. At position 1 of Fig. 2a (shown in Fig. 2a1), small bright nodules exist, which have an irregularly elongated shape and are oriented perpendicular to the fiber axis. At position 2 (shown in Fig. 2a2), the bright nodules are carved out more distinctly and seem to stick out of the fiber surface. Additionally, round black areas become visible, which represent holes within the fiber surface presumably produced by the starting solvation process. These holes are arranged in lines along the fiber axis and are located between two fibrils. Apparently, the dissolution process in the region of Fig. 2a2 has proceeded slightly faster than in the region of Fig. 2a1.

The FESEM image of Fig. 2b shows a PAN fiber at a presumably more advanced stage of etching. In contrast to Fig. 2a, the fiber surface is characterized by a much higher number of holes and only small regions of elongated nodules are left. Additionally, the lamella-like microstructure already known from Fig. 1d is found. The higher magnification image in Fig. 2b1 shows an area where these different stages of solvation coexist. Region 2 of Fig. 2b (shown in Fig. 2b2) is completely characterized by the lamellar microstructures, as found for completely separated rough fibrils of type II.

Based on the images of Fig. 2 the polymeric material in between the elongated nodules appears to be dissolved continuously by the proceeding etching process. Correspondingly, the nodules become more prominent, become thinner and develop the shape of fine layers, which are oriented perpendicular to the fiber axis. Due to the advanced solvation process holes develop.

It appears that the PAN material in between the lamella-like layers is dissolved faster by the DMSO

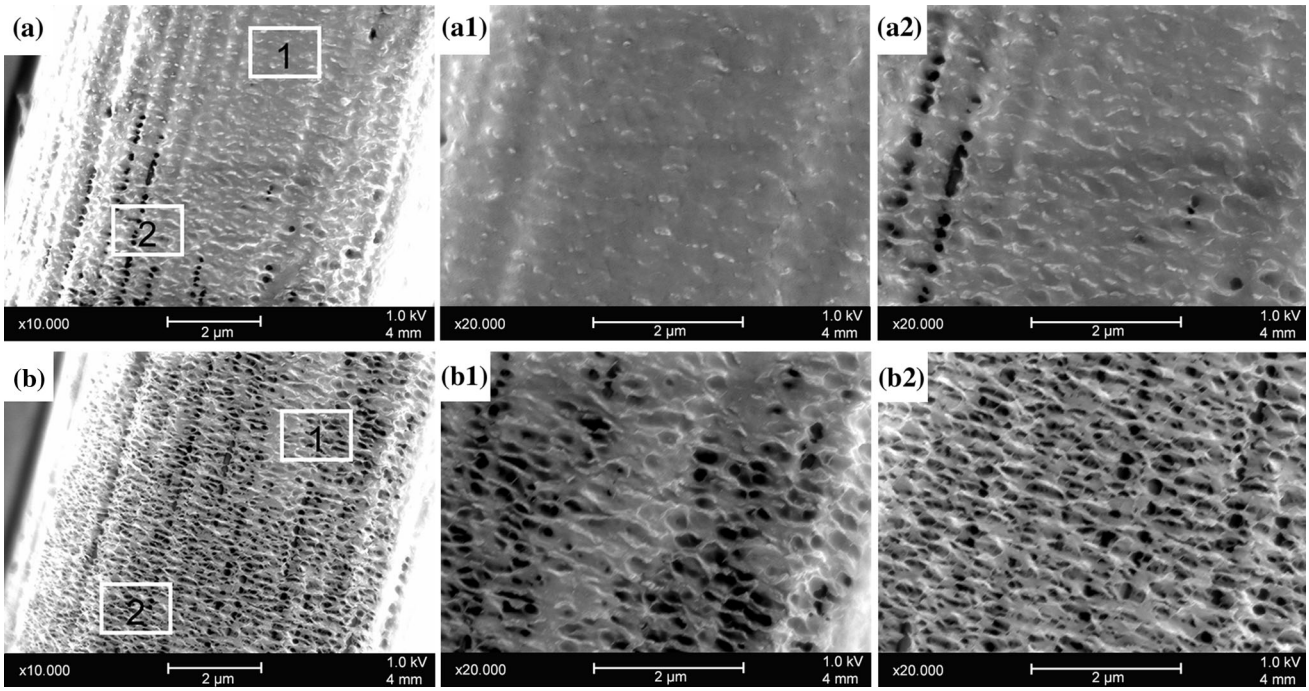

Figure 2 FESEM images of a PAN fiber surface at different dissolving states of ultrasonic etching, (**a**) surface at the beginning of etching (**a***1* + **a**2 at higher magnification), (**b**) surface at higher state of etching with a lamella-like framework (**b***1* + **b**2 at higher magnification).

solution than the layers themselves. As crystalline material is more resistant against solvation we assume, the layers consist of polymeric crystalline material, while the material in-between is amorphous in nature.

Nanoscale surface analysis of fibrils by AFM imaging

To obtain more detailed information on the surface morphology of the PAN fibrils on nanoscale, atomic force microscopy is used. For AFM, the tapping mode is an established method to analyze polymers. It has been shown by AFM that the surface of semicrystalline polymers has a nanoscale granular structure [56–59]. This granular structure is assumed to be caused by folding of polymer chains to small crystallites, separated by amorphous material in between [57, 60, 61].

Figure 3 shows AFM images of fibrils of type I and type II. For each fibril type, two different magnifications of AFM height images are shown. The white rectangles in Fig. 3a and c mark the areas of the corresponding high-magnification images in Fig. 3b and d, respectively. Figure 3a shows a fibril bundle of fibrils of type I. Individual fibrils of this bundle are marked by white arrows in Fig. 3b. In accordance with the previous FESEM investigations, fibrils of type I show a smooth surface morphology. The diameter of individual fibrils as determined by AFM amounts to 23 ± 7 nm (evaluation of 496 fibrils), which is smaller than that resulting from FESEM measurements. We suppose that due to insufficient contrast of the FESEM images several adjacent fibrils are falsely interpreted as one fibril. As AFM images provide a higher image contrast, the individual fibrils can be distinguished more clearly.

Figure 3c shows several individual fibrils of type II marked with white arrows. They show the typical lamella-like microstructure described above. The average diameter amounts to 461 ± 162 nm (evaluation of 11 fibrils), which is slightly higher but coincides within the margins of error with the value determined from FESEM images. Again, the lamella-like layers are oriented perpendicular to the fibril axis. In Fig. 3d, the lamellar structures are shown in higher magnification. Three lamella-like layers are marked by black arrows. The surfaces of the individual lamella-like layers are not smooth. Each layer is individually shaped and composed of granules with widths of around 20–80 nm. We interpret these granular structures as small polymer crystallites, which are not perfectly aligned relative to each other. Our AFM results are in accordance with the

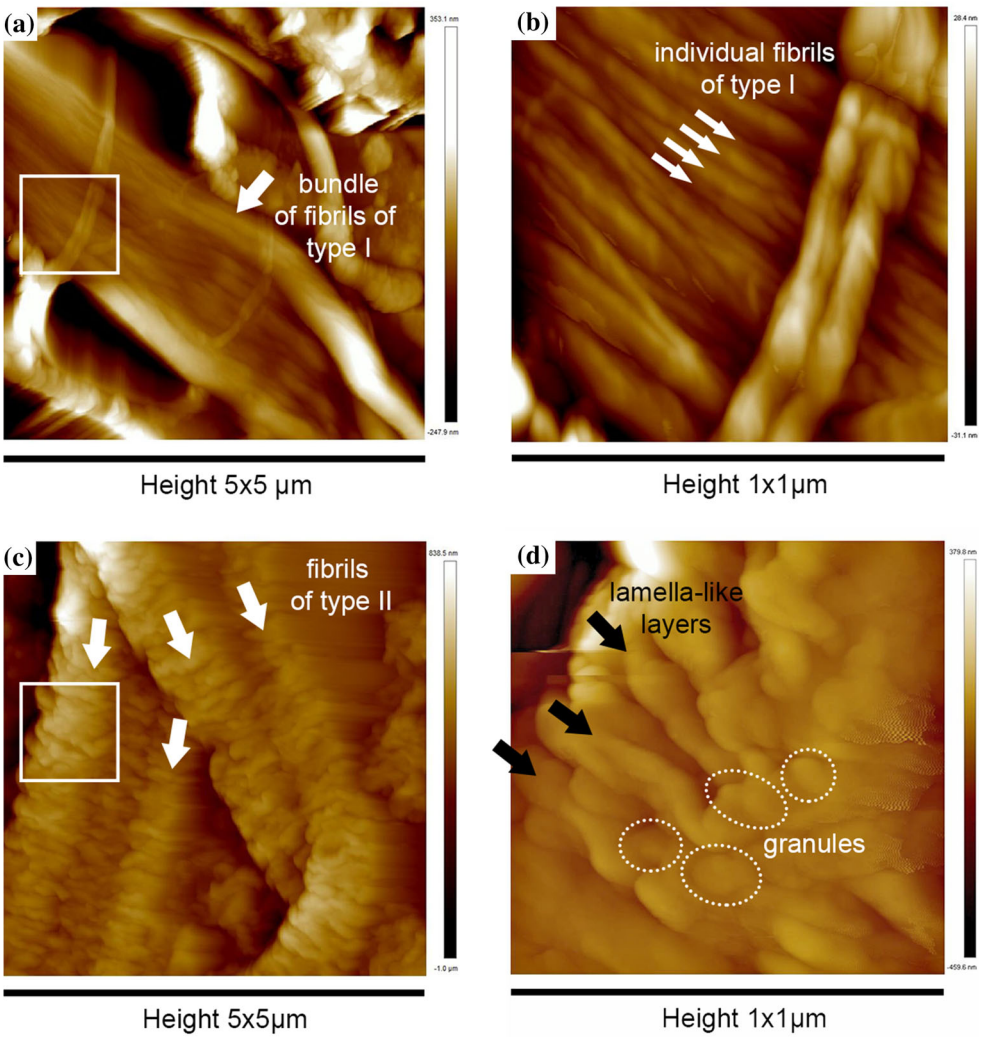

Figure 3 AFM height images of smooth fibrils of type I (**a**, **b**) and of rough fibrils of type II (**c**, **d**).

interpretation that lamella-like microstructures of fibrils of type II are crystalline.

Nanoscale bulk analysis of fibrils by TEM

To obtain information about the volume structure of the fibrils and to analyze the structural differences of the two types of fibrils, the samples were further analyzed by TEM. The TEM investigations shown in Fig. 4 support the FESEM and AFM results that two types of fibrils exist. In Fig. 4a, smooth fibrils of type I are shown, which are characterized by a low TEM contrast. The fibrils show an average diameter of 20 ± 11 nm (evaluation of 45 fibrils), which is similar to that determined by AFM measurements. Their volume structure is homogenous with no further substructures. The TEM image is typical for amorphous materials.

TEM images of fibrils of type II (Fig. 4b) show a complex substructure. In the center of the fibrils, which have an average diameter of 264 ± 102 nm (evaluation of 14 fibrils), a long string is found which is oriented along the fibril axis (in Fig. 4b from top left to bottom right). The string is clearly resolved by TEM, which, due to the transparency of the polymeric material for the electron beam, shows the projection of the complete fibril volume. In contrast, this string was not observed in the FESEM and AFM images, since here only the surface structure of the fibrils is resolved. To the best of our knowledge, this is the first time that such kind of string is observed within PAN fibrils. These strings exhibit an average diameter of 26 ± 17 nm. Perpendicular to the string, filigree lamella-like substructures are clearly visible, which are characterized by a thickness of 10 ± 4 nm (evaluation of 72 lamella-like layers) and seem to

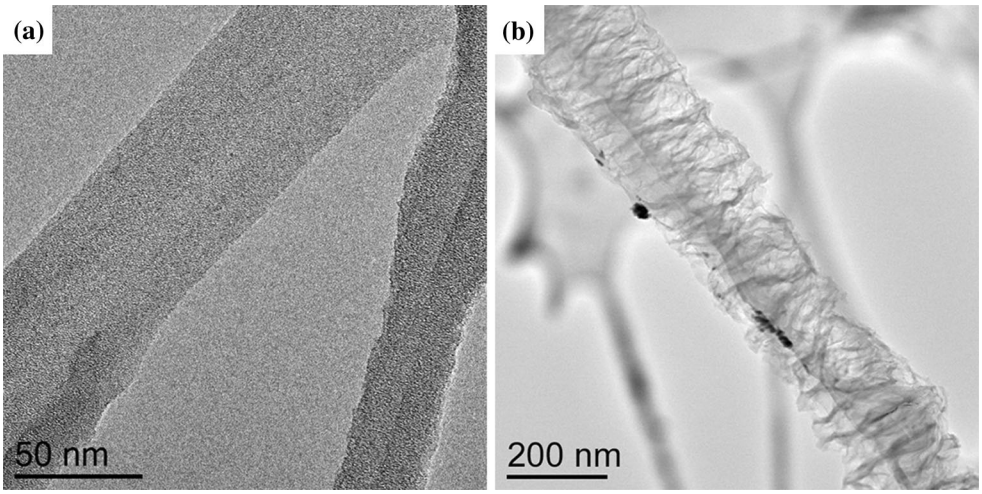

Figure 4 TEM images of **a** smooth (type I) and **b** lamella-like fibrils (type II).

surround the string. The lamella-like substructures were detected already by FESEM and AFM analysis, where they are responsible for the rough surface morphology of the fibrils of type II. The thickness of these lamella-like structures appears smaller in the TEM measurements, because only material with sufficiently high TEM contrast was considered for the thickness measurements. A high TEM contrast can be due to density differences, thickness differences or variations in crystallinity and crystallite orientation. We assume that the lamella-like structures of the rough fibrils are crystalline. This is consistent with the results described above, namely the etching behavior of the fibrils and the granular structure of the lamella-like layers.

The dimensions of the observed fibril substructures as measured by TEM are summarized in the diagram of Fig. 5. The smooth fibrils of type I have the smallest diameter of 20 ± 11 nm, which is similar to the diameter of the string of type II fibrils of 26 ± 17 nm. The diameter of the fibrils of type II amounts to 264 ± 102 nm. Their lamellar-like layers exhibit a thickness of only 10 ± 4 nm and arrange perpendicular to the fibril axis.

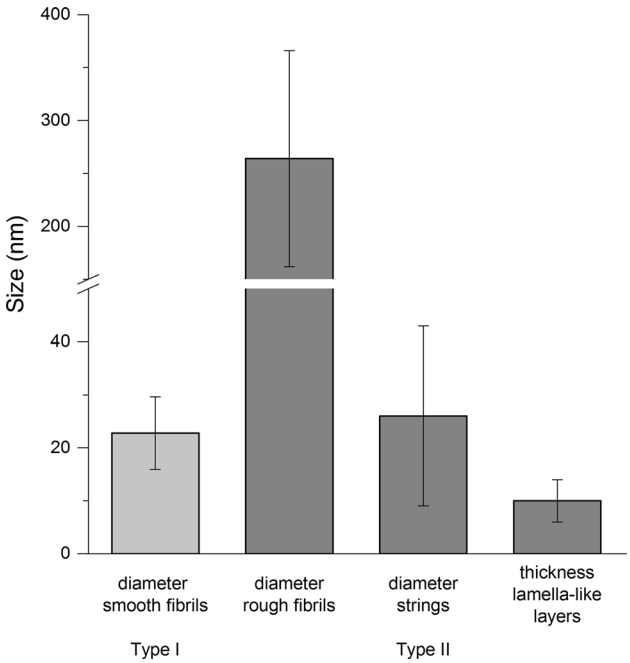

Figure 5 Dimensions of two types of PAN fibrils and their substructures.

Comparison of fibril morphology of technical and textile PAN fibers

All investigations described so far were performed on the technical PAN fiber A. To elucidate the influence of the PAN fiber type on the fibril morphology, additionally two other PAN fiber types (PAN B and PAN C) were analyzed. PAN B is also a technical PAN fiber, while PAN C is used for textile applications. The character of the three PAN fiber types is defined by their crystalline properties, which were analyzed by XRD. The qualitative results of the XRD analysis are shown in Table 1. The three PAN fiber types differ in their crystallinity, crystallite size, and crystallite orientation. The crystallinity, the crystallite size, and the orientation of the PAN crystallites decreases in the following order: PAN A > PAN B > PAN C.

Table 1 Relative degree of crystallinity, crystallite size, and crystallite orientation of the three types of PAN fibers

Specimen type	Crystallinity	Crystallite size	Crystallite orientation
PAN A	High	High	High
PAN B	Intermediate	Intermediate	Intermediate
PAN C	Low	Low	Low

The fibers PAN B and PAN C were prepared in accordance with PAN A in DMSO solution in the USB to separate them into their fibrils. The resulting material was analyzed using FESEM. A test series with different concentrations of the DMSO solution was performed to identify the optimal parameters for each PAN fiber type. Table 2 summarizes the DMSO concentrations used. The values highlighted in italics are concentrations, which are too low for the respective type of fiber and did not result in fibril separation. In contrast, the concentrations highlighted in bold are too high and resulted in complete dissolution of the fibers. The optimal concentrations for the separation of the respective fibers into their fibrils are the remaining ones which are underlined.

A clear correlation between the crystalline properties and the dissolution behavior is observed. The higher the crystallinity, the crystallite size and the crystallite orientation of the fiber, the higher the concentration of DMSO necessary to separate the fibers into their fibrils. From the data, it cannot be decided which of the crystallite properties determines the solvation behavior.

For all three types of fibers, both smooth and rough fibrils are found. However, the ratio of these two fibril types depends on the fiber character. Samples of PAN B and C show less rough fibrils of type II than samples of PAN A. The amount of fibrils of type II decreases in the order PAN A > PAN B > PAN C, i.e., the crystallinity is correlated to the number of type II fibrils.

Table 2 DMSO concentration used for ultrasonic etching of the three types of PAN fibers

Specimen type	DMSO concentration (%)			
PAN A	*80*	*85*	90	95
PAN B	*80*	85	90	**95**
PAN C	80	85	**90**	**95**

Discussion

Based on the microscopic investigations, we suggest a structural model of the PAN fiber where the two types of fibrils coexist. Figure 6 shows schematically the structural relation between the type I and type II fibrils.

Type I fibrils have a smooth surface and a homogeneous volume structure. Such fibrils are described in literature [27]. They are formed by stretched polymer chains, which are oriented preferentially parallel to each other. Stretching of the polymer chains and their orientation along the fibril and fiber axis can occur during the spinning and stretching process of the PAN fibers [27, 62]. Although no crystalline regions were detected, the smooth fibrils show a higher resistance to the solution process than the surrounding amorphous material. We assume that this resistance results from the increased intermolecular forces between the parallel-aligned molecule chains.

In contrast, type II fibrils are characterized by lamella-like layers arranged perpendicular to a central string. In literature, this arrangement is referred to as shish-kebab structure and is typical for polymer crystallization under shear flow stress or under uniaxial tension [37, 63]. Such a structure is also found in other polymer fibers, e.g., polyethylene or polypropylene fibers [64–66]. Its existence is attributed to shear conditions during the spinning process of such fibers. The molecular chains of the polymer are stretched, arrange parallel to each other and form shish structures, similar to type I fibrils [67]. Growth of the kebab structure takes place at those parts of the shish, where the polymer chains are particularly well oriented [62, 68]. These well-aligned areas of the shish represent nuclei for crystallization of the kebab structures and define the direction of their growth perpendicular to the direction of the shish [35, 62, 68]. The kebab structures in turn consist of the sheet-like arrangement of polymer crystallites formed from folded molecular chains. We identify these kebab

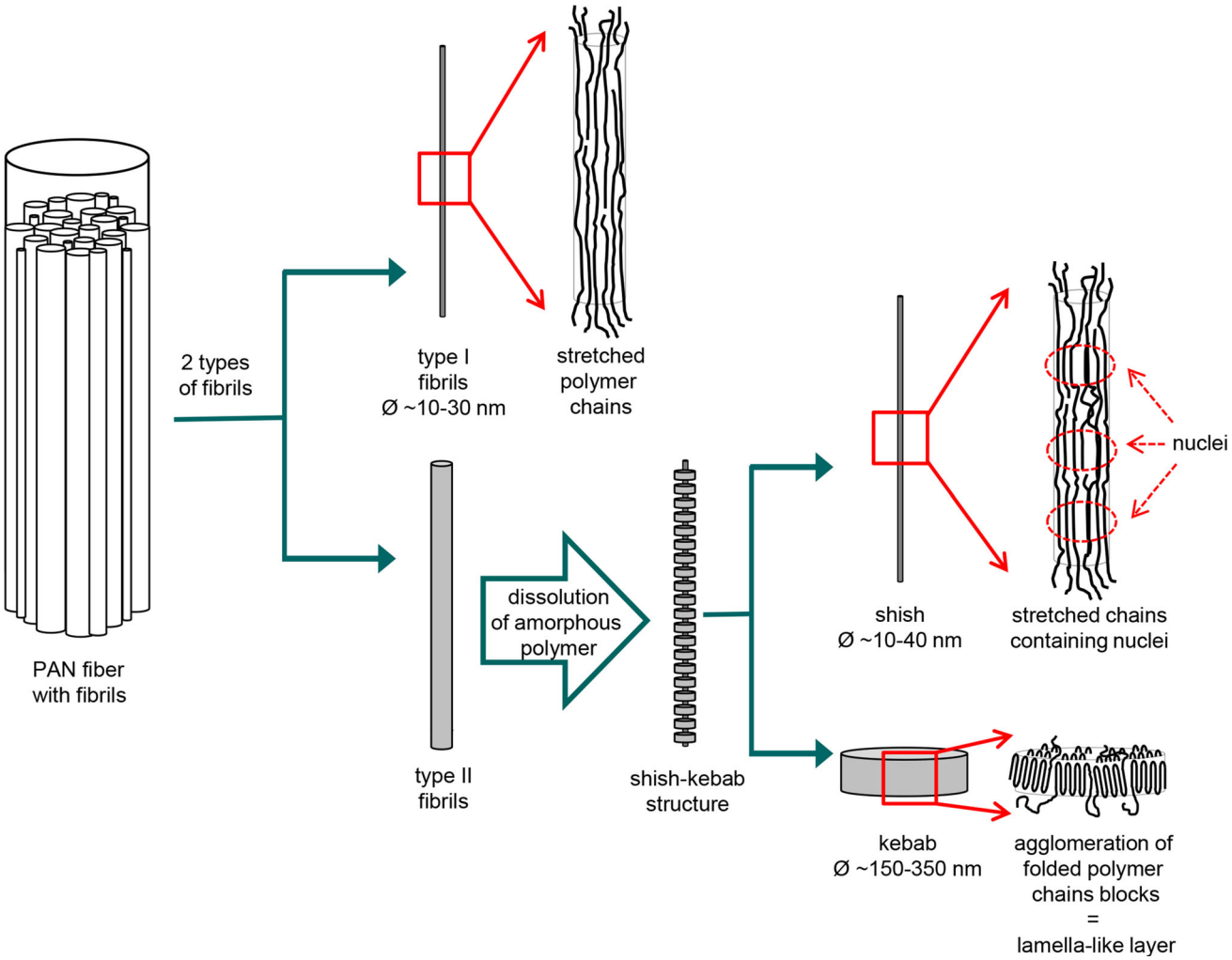

Figure 6 Schematic model of the fibril structures of PAN fibers and the differences between the two fibril types.

structures with our lamella-like layers and the shish structure with our strings within the type II fibrils. The lamella-like layers with a granular surface structure, as detected by AFM, are interpreted as a result of the agglomeration of small polymer crystallites, which are not perfectly oriented with respect to each other and connected by amorphous regions [69].

Conclusion

Technical and textile PAN fibers were separated into their fibrils by ultrasonic etching. In all types of PAN fibers, two different fibril morphologies were found. On the one hand, fibrils with smooth surface and homogeneous, amorphous volume structure exist (type I). On the other hand, fibrils with the typical shish-kebab structure are found (type II), characterized by crystalline lamella-like layers oriented perpendicular to a centered shish. As the diameter of this shish is similar to the diameter of the smooth fibrils, the smooth fibril is assumed to be the nucleus for crystallization of lamella-like structures and, therefore, the formation of type II fibrils. The growth of lamella-like crystalline layers occurs probably at well-ordered surface regions of smooth fibrils. This results in the coexistence of smooth and rough fibrils within one PAN fiber. With increasing crystallinity of the PAN fibers, the relative amount of shish-kebab fibrils of type II increases, thus representing an indicator for the character of the PAN fibers.

Compliance with ethical standards

Conflict of interest The authors declare that they have no conflict of interest.

References

[1] Olabisi O, Adewale K (2016) Handbook of Thermoplastics. CRC Press, Taylor & Francis Group, Boca Raton

[2] Masson JC (ed) (1995) Acrylic fiber technology and applications. M. Dekker, New York

[3] Morita K, Murata Y, Ishitani A, Murayama K, Ono T, Nakajima A (1986) Characterization of commercially available PAN (polyacrylonitri1e)-based carbon fibers. Pure Appl Chem 58(3):455–468

[4] Damodaran S, Desai P, Abhiraman AS (2008) Chemical and physical aspects of the formation of carbon fibres from PAN-based precursors. J Text Inst 81(4):384–420

[5] Frank E, Steudle LM, Ingildeev D, Spörl JM, Buchmeiser MR (2014) Carbon fibers: precursor systems, processing, structure, and properties. Angew Chem Int Ed 53(21):5262–5298

[6] Fitzer E (1989) Pan-based carbon fibers—present state and trend of the technology from the viewpoint of possibilities and limits to influence and to control the fiber properties by the process parameters. Carbon 27(5):621–645

[7] Chand S (2000) Review: carbon fibers for composites. J Mater Sci 35(6):1303–1313. https://doi.org/10.1023/A:1004780301489

[8] Ruland W (1990) Carbon fibers. Adv Mater 2(11):528–536

[9] Perret R, Ruland W (1970) The microstructure of PAN-base carbon fibres. J Appl Crystallogr 3(6):525–532

[10] Qian X, Zou R, OuYang Q, Wang X, Zhang Y (2015) Surface structural evolvement in the conversion of polyacrylonitrile precursors to carbon fibers. Appl Surf Sci 327:246–252

[11] Li W, Long D, Miyawaki J, Qiao W, Ling L, Mochida I, Yoon S (2012) Structural features of polyacrylonitrile-based carbon fibers. J Mater Sci 47(2):919–928. https://doi.org/10.1007/s10853-011-5872-2

[12] Edie DD (1998) The effect of processing on the structure and properties of carbon fibers. Carbon 36(4):345–362

[13] Wangxi Z, Jie L, Gang W (2003) Evolution of structure and properties of PAN precursors during their conversion to carbon fibers. Carbon 41(14):2805–2812

[14] Fitzer E, Frohs W, Heine M (1986) Optimization of stabilization and carbonization treatment of PAN fibres and structural characterization of the resulting carbon fibres. Carbon 24(4):387–395

[15] Bajaj P, Munuktla Surya Kumari, Vaidya AA, Gupta DC (1989) Influence of spinning dope additives and spin bath temperature on the structure and physical properties of acrylic fibers. Text Res J 59(10):601–608

[16] Fitzer E, Frohs W (1990) Modern carbon fibres from polyacrylonitrile (PAN)-polyheteroaromatics with preferred orientation. Chem Eng Technol 13(1):41–49

[17] Wilms C, Seide GH, Gries T (2013) The relationship between process technology, structure development and fibre properties in modern carbon fibre production. Chem Eng Trans 32:1609–1614

[18] Park S (2015) Carbon Fibers. Springer Series in Materials Science 210. Springer, Dordrecht

[19] Arbab S, Noorpanah P, Mohammadi N, Soleimani M (2008) Designing index of void structure and tensile properties in wet-spun polyacrylonitrile (PAN) fiber. I. Effect of dope polymer or nonsolvent concentration. J Appl Polym Sci 109(6):3461–3469

[20] Knudsen JP (1963) The influence of coagulation variables on the structure and physical properties of an acrylic fiber. Text Res J 33(1):13–20

[21] Cahn JW (1965) Phase separation by spinodal decomposition in isotropic systems. J Chem Phys 42(1):93–99

[22] Arbab S, Noorpanah P, Mohammadi N, Soleimani M (2008) Designing index of void structure and tensile properties in wet-spun polyacrylonitrile (PAN) fiber. I. Effect of dope polymer or nonsolvent concentration. J Appl Polym Sci 109(6):3461–3469

[23] Bell JP, Dumbleton JH (1971) Changes in the structure of wet-spun acrylic fibers during processing. Text Res J 41(3):196–203

[24] van de Witte P, Dijkstra PJ, van den Berg J, Feijen J (1996) Phase separation processes in polymer solutions in relation to membrane formation. J Membr Sci 117(1–2):1–31

[25] Tucker P, George W (1972) Microfibers within fibers: a review. Polym Eng Sci 12(5):364–377

[26] Craig JP, Knudsen JP, Holland VF (1962) Characterization of acrylic fiber structure. Text Res J 32(6):435–448

[27] H. Zahn (1986) Neues über den Feinbau von Textilfasern (60):7–18

[28] Sawyer L, George W (1985) Evolution of fibrous structures within unstable polymeric fluids. Text Res J 55:415–424

[29] Warner SB, Uhlmann DR (1979) Oxidative stablzation of acrylic fibres. J Mater Sci 14(8):1893–1900. https://doi.org/10.1007/BF00772715

[30] Hinrichsen G (1972) Structural changes of drawn polyacrylonitrile during annealing. J Polym Sci C Polym Symp 38(1):303–314

[31] Hermann K, Gerngross O, Abitz W (1930) X-ray studies of the structure of gelatin micelles. Zeitschrift für Physikalische Chemie (Abteilung B) 10:371–394
[32] Hearle JWS (1958) A fringed fibril theory of structure in crystalline polymers. J Polym Sci 28(117):432–435
[33] Keller A (1957) A note on single crystals in polymers: evidence for a folded chain configuration. Phil Mag 2(21):1171–1175
[34] Lauritzen JI, Hoffman JD (1960) Theory of formation of polymer crystals with folded chains in dilute solution. J Res Natl Bur Stand A 64(1):73–102
[35] Hoffmann JD, Lauritzen JK (1961) Crystallization of bulk polymer with chain folding: theory of growth of lamellar spherulites. J Res Natl Bur Stand Sect A 65(4):297–336
[36] Somani RH, Yang L, Zhu L, Hsiao BS (2005) Flow-induced shish-kebab precursor structures in entangled polymer melts. Polymer 46(20):8587–8623
[37] Pennings AJ (1980) Polymer crystallization. J Cryst Growth 48(4):574–581
[38] Carraher CE, Seymour RB (2003) Seymour/Carraher's polymer chemistry, 6th edn. Undergraduate chemistry 16. Dekker, New York
[39] Keith HD, Padden FJ Jr (1963) A phenomenological theory of spherulitic crystallization. J Appl Phys 34(8):2409–2421
[40] Keller A (1979) Crystalline polymers; an introduction. Faraday Discuss Chem Soc 68:145–166
[41] Yoon DY, Flory PJ (1979) Molecular morphology in semicrystalline polymers. Faraday Discuss Chem Soc 68:288–296
[42] Yoon DY, Flory PJ (1977) Small-angle neutron scattering by semicrystalline polyethylene. Polymer 18(5):509–513
[43] Gupta AK, Paliwal DK, Bajaj P (1991) Acrylic precursors for carbon fibers. Polymer Revs 31(1):1–89
[44] Johnson DJ, Tyson CN (1969) The fine structure of graphitized fibres. J Phys D Appl Phys 2(6):787–795
[45] Wang Q, Wang C, Bai Y, Yu M, Wang Y, Zhu B, Jing M, Ma J, Hu X, Zhao Y, Zhang M (2010) Fibrils separated from polyacrylonitrile fiber by ultrasonic etching in dimethyl-sulphoxide solution. J Polym Sci Polym Phys 48(5):617–619
[46] Wang Q, Wang C, Yu M, Ma J, Hu X, Zhu B, Wang C, Yu M, Hu X (2010) Microstructure of fibrils separated from polyacrylonitrile fibers by ultrasonic etching. Sci China Technol Sci 53(6):1489–1494
[47] C. Kunzmann, J. Moosburger-Will, S. Horn (2015) In: C. Kunzmann, J. Moosburger-Will, S. Horn (ed) Microscopic investigation of the micro-structure of fibrils of technical poylacrylonitrile fibers separated by ultrasonic etching
[48] Wang S, Cheng Q (2009) A novel process to isolate fibrils from cellulose fibers by high-intensity ultrasonication, part 1: process optimization. J Appl Polym Sci 113(2):1270–1275
[49] Yu M, Xu Y, Wang C, Hu X, Zhu B, Qiao K, Yuan H (2012) Heredity and difference of multiple-scale microstructures in PAN-based carbon fibers and their precursor fibers. J Appl Polym Sci 125(4):3159–3166
[50] Cheng Q, DeVallance D, Wang J, Wang S (2011) Advanced Cellulosic Nanocomposite Materials
[51] Ohhashi Y, Kihara M, Naiki H, Goto Y (2005) Ultrasonication-induced amyloid fibril formation of beta 2-microglobulin. J Biol Chem 280(38):32843–32848
[52] Fan J, Yu W (2009) Basic parameter study for the separation of wool fibre components by ultrasonic irradiation in formic acid. Text Appar 13(2):69–74
[53] Gardner KH, Blackwell J (1971) The substructure of the cellulose microfibrils from the cell walls of the algae Valonia ventricosa. J Ultrastruct Res 36(5–6):725–731
[54] Shirahama T (1967) High-resolution electron microscopic analysis of the amyloid fibril. J Cell Biol 33(3):679–708
[55] Frenzel R, Moosburger-Will J, Horn S (2015) In: Frenzel R, Moosburger-Will J, Horn S (eds) Evolution of crystalline parameters during stabilization of polyacrylontitrile fibers
[56] Hugel T, Strobl G, Thomann R (1999) Building lamellae from blocks: the pathway followed in the formation of crystallites of syndiotactic polypropylene. Acta Polym 50(5–6):214–217
[57] Strobl G (2009) Colloquium: laws controlling crystallization and melting in bulk polymers. Rev Mod Phys 81(3):1287–1300
[58] Ogawa T, Miyaji H, Asai K (1985) Nodular structure of polypropylene. J Phys Soc Jpn 54(10):3668–3670
[59] Zia Q, Radusch HJ, Androsch R (2010) AFM study of the nanostructure of quenched isotactic polypropylene. Microsc Sci Technol Appl Educ 3:1940–1950
[60] Hobbs JK, Farrance OE, Kailas L (2009) How atomic force microscopy has contributed to our understanding of polymer crystallization. Polymer 50(18):4281–4292
[61] Loos J, Thüne PC, Niemantsverdriet JW, Lemstra PJ (1999) Polymerization and crystallization of polyethylene on a flat model catalyst. Macromolecules 32(26):8910–8913
[62] Somani RH, Yang L, Hsiao BS, Agarwal PK, Fruitwala HA, Tsou AH (2002) Shear-induced precursor structures in isotactic polypropylene melt by in-situ rheo-SAXS and rheo-WAXD studies. Macromolecules 35(24):9096–9104
[63] Keller A (1977) A current account of chain extension, fibrous crystallization, and fiber formation. J Polym Sci C Polym Symp 58(1):395–422
[64] Liu S, Zhang F, Zheng G, Dai K, Liu C, Shen C, Guo JZ (2016) Direct microscopic observation of shish-kebab structure in high-temperature electrospun iPP fibers. Mater Lett 172:149–152

[65] Ohta Y, Murase H, Hashimoto T (2010) Structural development of ultra-high strength polyethylene fibers: transformation from kebabs to shishs through hot-drawing process of gel-spun fibers. J Polym Sci Part B Polym Phys 48(17):1861–1872

[66] Hoogsteen W, Hooft RJ, Postema AR, Gt Brinke, Pennings AJ (1988) Gel-spun polyethylene fibres. J Mater Sci 23(10):3459–3466. https://doi.org/10.1007/BF00540479

[67] Pennings AJ, van der Mark J, Kiel Am (1970) Hydrodynamically induced crystallization of polymers from solution. Colloid Polym Sci 237(2):336–358

[68] Hu W, Frenkel D, Mathot VBF (2002) Simulation of shish-kebab crystallite induced by a single prealigned macromolecule. Macromolecules 35(19):7172–7174

[69] Guttman CM, DiMarzio EA, Hoffman JD (1981) Modelling the amorphous phase and the fold surface of a semicrystalline polymer—the Gambler's Ruin method/Modelling the amorphous phase and the fold surface of a semicrystalline polymer?: The Gambler's Ruin method. Polymer 22(11):1466–1479